Speciation and Reactivity Control of Cu-Oxo Clusters via Extraframework Al in Mordenite for Methane Oxidation

Tao, Lei; Khramenkova, Elena; Lee, Insu; Ikuno, Takaaki; Khare, Rachit; Jentys, Andreas; Fulton, John L.; Kolganov, Alexander A.; Pidko, Evgeny A.; Sanchez-Sanchez, Maricruz

DOI
10.1021/jacs.3c04328

Publication date
2023

Document Version
Final published version

Published in
Journal of the American Chemical Society

JACS
JOURNAL OF THE AMERICAN CHEMICAL SOCIETY
pubs.acs.org/JACS
Article

Speciation and Reactivity Control of Cu-Oxo Clusters via Extraframework Al in Mordenite for Methane Oxidation

Lei Tao,[⊥] Elena Khramenkova,[⊥] Insu Lee, Takaaki Ikuno, Rachit Khare, Andreas Jentys, John L. Fulton, Alexander A. Kolganov, Evgeny A. Pidko,* Maricruz Sanchez-Sanchez,* and Johannes A. Lercher*

Cite This: J. Am. Chem. Soc. 2023, 145, 17710−17719

ABSTRACT: The stoichiometric conversion of methane to methanol by Cu-exchanged zeolites can be brought to highest yields by the presence of extraframework Al and high CH_4 chemical potentials. Combining theory and experiments, the differences in chemical reactivity of monometallic Cu-oxo and bimetallic Cu-Al-oxo nanoclusters stabilized in zeolite mordenite (MOR) are investigated. Cu-L_3 edge X-ray absorption near-edge structure (XANES), infrared (IR), and ultraviolet−visible (UV−vis) spectroscopies, in combination with CH_4 oxidation activity tests, support the presence of two types of active clusters in MOR and allow quantification of the relative proportions of each type in dependence of the Cu concentration. *Ab initio* molecular dynamics (MD) calculations and thermodynamic analyses indicate that the superior performance of materials enriched in Cu-Al-oxo clusters is related to the activity of two μ-oxo bridges in the cluster. Replacing H_2O with ethanol in the product extraction step led to the formation of ethyl methyl ether, expanding this way the applicability of these materials for the activation and functionalization of CH_4. We show that competition between different ion-exchanged metal-oxo structures during the synthesis of Cu-exchanged zeolites determines the formation of active species, and this provides guidelines for the synthesis of highly active materials for CH_4 activation and functionalization.

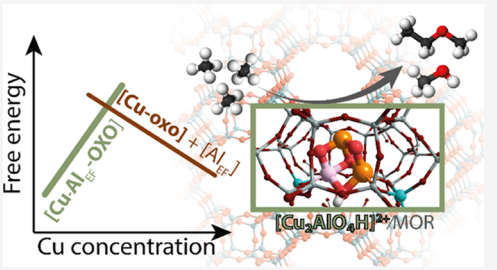

INTRODUCTION

Methane has emerged over the last decade as the key feedstock for the transition to a carbon-neutral chemical and refining industry.[1−3] Among the different transformation routes, the direct conversion of methane to methanol represents one of the most enticing, yet challenging pathways. Due to the perceived need to apply severe reaction conditions to cleave at least one of the C−H bonds, very low methanol yields are typically obtained.[4,5]

Inspired by the naturally occurring particulate methane monooxygenases (pMMO),[6−9] copper-exchanged zeolites have been developed as selective methane to methanol catalysts following a three-stage process that uses air as oxidant. Multiple zeolite topologies have been shown to accommodate active cationic Cu-oxo clusters for the transformation, among which mordenite (MOR) is arguably the most widely studied zeolite. Spectroscopic characterization of these materials has led to different and, at times, conflicting proposals of the geometry of the active sites in zeolites. Most reports have found dimeric or trimeric Cu-oxo clusters as the active sites in Cu-MOR.[10−20] Numerous material and synthesis parameters have been identified as relevant in directing the structure of Cu-oxo clusters, including the presence of other cations in the parent zeolite,[15,21] the distribution of the framework aluminum,[22,23] and the ion exchange procedure.[11,24] The ability of Cu-oxo clusters to activate CH_4 also depends on the geometry and size of the pores as well as the local environment.[12,22,25−28] Understanding of the speciation of Cu ions and charged Cu-oxo clusters has been found also to be relevant for other redox catalytic applications such as NH_3 selective catalytic reduction of NO_x.[29,30] All of these spectroscopic, theoretical, and catalytic studies of Cu-oxo clusters have opened new possibilities for the synthesis of structures capable to stabilize active oxygen species.

Recently, the presence of extraframework Al (EFAl) has been found to increase the activity of Cu-MOR materials in methane oxidation.[24,31] The combination of spectroscopic and computational studies links the origin of such activity increase to the formation of active Cu_2AlO_3 clusters by the reaction of the Cu ions with EFAl species located near the bottom of the 8 MR side pockets.[31] The formation of such Cu-Al-oxo clusters leads to higher productivity per Cu than clusters formed with only Cu. This study investigates the increase in methane oxidation activity observed for Cu-MOR materials—synthesized by methods that leads to the predominant formation of

Received: April 26, 2023
Published: August 7, 2023

https://doi.org/10.1021/jacs.3c04328
J. Am. Chem. Soc. 2023, 145, 17710−17719

$[Cu_3O_3]^{2+}$ clusters[15,16]- when EFAl species are present inside the micropores. The Cu_2AlO_3 core structure as previously described[31] is further stabilized by an additional OH group. Methane oxidation tests are performed at a wider range of methane pressures, revealing the upper limit in the number of active oxygen atoms that Cu-oxo and Cu-Al-oxo clusters can utilize to convert CH_4. *Ab initio* thermodynamic analysis (aiTA) and molecular dynamics (MD) combined with spectroscopic methods reveal a dynamic equilibrium between Cu-oxo and Cu-Al-oxo cluster structures, both active in methane oxidation, determined by the concentration of Cu ions and EFAl available during ion exchange. The reaction of CH_4-loaded Cu-MOR materials with ethanol sheds light on the differences in the reactivity of CH_x− surface intermediates, which are related to either electronic differences or environmental constraints of the clusters. Furthermore, this strategy constitutes a novel pathway to generate methyl-based ether compounds from CH_4.

RESULTS AND DISCUSSION

Oxidative Conversion of CH_4 over Cu-Al-Oxo Clusters Hosted in MOR. Prior to this study, we synthesized and reported on a series of Cu-MOR materials with a capacity to activate ca. 0.6 molecules of CH_4 per Cu atom, in a typical three-stage process of methane oxidation at 1 bar. The selectivity to methanol was in all cases in the range of 65 to 85%. This high Cu efficiency (Cu_{eff}, defined as the molar ratio of converted methane to the total Cu content) is attributed to the formation of highly active Al-containing clusters by the reaction of exchanged Cu ions with EFAl species entrained in the zeolite pores.[31] On the other hand, it has been shown that Cu-MOR materials can reach significantly higher Cu_{eff} under high methane pressures (ca. 40 bar).[13,17,32] This has been attributed to the fact that, at high CH_4 chemical potential, a second oxygen atom from a Cu-oxo active cluster becomes active for methane oxidation.[10,17] In order to determine whether the reactivity of Cu-Al-oxo clusters could be increased at high CH_4 chemical potentials, we studied the activity of an EFAl-containing Cu-MOR series at 40 bar and compared it to activity at 1 bar. As shown in Figure 1, the total yields achieved at 40 bar of methane pressure increased by at least 10%. However, the increase is significantly smaller than the ca. 100% activity increase we had previously achieved for Cu-MOR materials containing solely $[Cu_3O_3]^{2+}$ clusters.[16,17] This shows that the response to the CH_4 chemical potential of Cu-Al-oxo clusters is different from that of pure Cu-oxo clusters. It should be noted that this is true for samples in the Cu-MOR series with low to medium Cu concentrations. However, for Cu loadings above 400 μmol/g, we observed an increase in methanol yields of nearly 100% when increasing pressure from 1 to 40 bars, similar to the Cu-MOR series containing only Cu-oxo species. This is the first indication of a complex Cu speciation in the presence of EFAl, likely because different Cu-oxo structures are formed, in dependence of the Cu concentration available during ion exchange.

In a different experiment, we subjected the Cu-MOR materials to a treatment with ethanol instead of water, after reacting CH_4, in order to extract the reaction products. While water is known to hydrolyze and solvate the Cu-oxo clusters during the methanol desorption stage,[16] ethanol on the other hand is expected to dehydrate to diethyl ether on the zeolite and form ethyl methyl ether (EME) with the CH_3 moiety without affecting Cu structure. This, together with the larger molecular diameter of ethanol in comparison to H_2O will contribute to determining the location and reactivity of surface-activated CH_x groups.

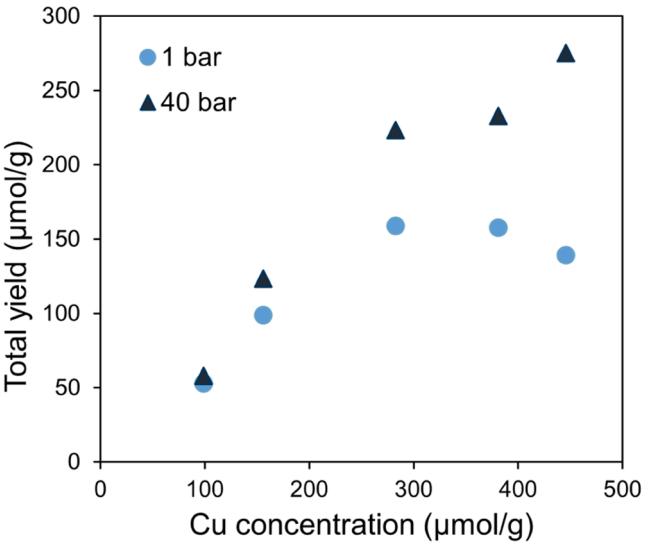

Figure 1. Total yields achieved on Cu-MOR series after activation in O_2 at 500 °C for 1 h, followed by reaction in CH_4 flow at 200 °C (at 1 or 40 bar) for 3 h and subsequent treatment in 20% H_2O/He flow at 135 °C.

After the CH_4 reaction, treating the activated Cu-MOR with ethanol produced small concentrations of EME as the only product apart from diethyl ether. EME is an important asymmetrical ether, which is commonly accessible via synthetic methods involving using highly toxic methyl iodide. Using Cu-MOR materials, however, EME (and potentially other methyl ethers) can be formed from merely CH_4, O_2, and the corresponding alcohol, which follows an S_N2-type reaction between the alcohol molecules and the surface methoxy groups. In Figure 2, it can be seen that the EME yield increased monotonically with the Cu concentration in the zeolite, up to the sample containing 380 μmol/g of Cu. Interestingly, EME yields are approximately 75% of the methanol yields obtained in reaction with H_2O. Only on those samples with Cu loadings above 300 μmol/g we quantify similar amounts of EME and methanol yields in corresponding activity tests. Based on this,

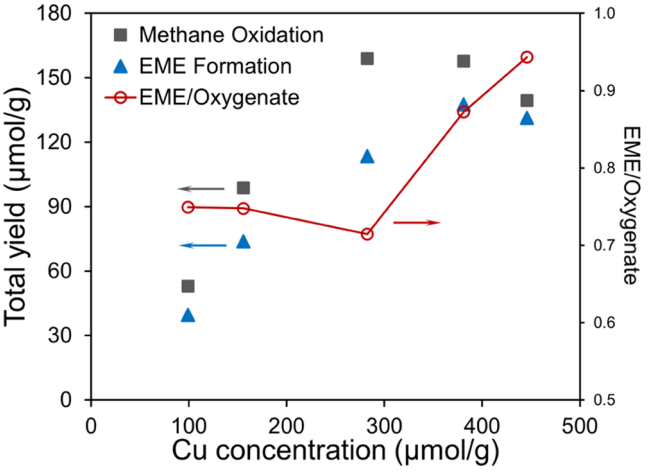

Figure 2. EME yields achieved on Cu-MOR series and the ratio if normalized to methanol yields.

https://doi.org/10.1021/jacs.3c04328
J. Am. Chem. Soc. 2023, 145, 17710−17719

we speculate that the cluster structures formed at low Cu loadings have specific nature or location that renders them less reactive to EtOH than to H_2O. This observation, in agreement with the observed activity increase at high CH_4 chemical potentials (Figure 1), indicates that Cu speciation changes with Cu concentration for EFAl-containing MOR materials, in contrast to the homogeneous speciation observed for Cu-MOR materials in the absence of EFAl.[16] In particular, our results point to two different Cu speciation regions with a transition occurring at a Cu concentration of ca. 300 μmol/g.

Based on our previous studies on Cu clusters in MOR,[17,31] we hypothesize that EFAl-containing MOR materials form both Cu-Al-oxo and Cu-oxo clusters, and their concentrations are determined by the availability of Cu ions and EFAl species during ion exchange. Therefore, the activity of Cu-MOR is expected to be quantitatively related to the concentrations of clusters with Cu-Al-oxo bimetallic[31] and pure Cu-oxo species structures.[16] A modest increase of activity with CH_4 pressure, as seen for low Cu loading samples in Figure 1, is indicative of a large proportion of Cu forming Al-containing clusters because such cluster has already reached its activity upper limit at 1 bar, activating two CH_4 molecules.[31] Conversely, it is known that $[Cu_3O_3]^{2+}$ clusters activate ca. 1 CH_4 molecule at 1 bar[16] and 2 CH_4 molecules at 40 bar.[17] Based on these CH_4-to-cluster stoichiometries, and assuming that only these two types of clusters participate in the reaction, the concentrations of each of the two clusters can be calculated from the Cu concentration and the total yields of CH_4 to CH_3OH reaction at 1 bar (see Section S3 in the Supporting information). As shown in Figure 3, materials with Cu concentrations below 300

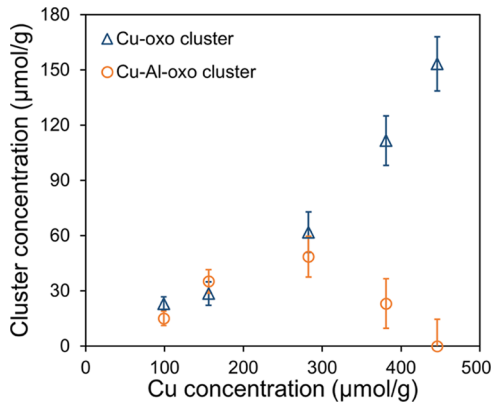

Figure 3. Distribution of Cu-oxo and Cu-Al-oxo clusters in EFAl-containing Cu-MOR materials, calculated based on the assumption of 1 CH_4 activated per Cu-oxo cluster containing 3 Cu and 1 CH_4 activated per Cu-Al-oxo cluster containing 2 Cu, and the experimental yields obtained for selective methane oxidation at 1 bar (see Section S3 for calculation details).

μmol/g contain approximately 50% of each type of cluster, while the proportion of the Cu-oxo cluster significantly increases at higher Cu concentrations, at the expense of the Cu-Al-oxo cluster.

In order to test the experimentally induced concentration of each type of cluster, we studied the thermodynamic stability of the Cu-oxo and Cu-Al-oxo clusters at different Cu concentrations with DFT-based aiTA. The stability of the respective models and their potential reactivity toward the sequential activation of several methane molecules were studied utilizing the periodic spin-polarized calculations at the PBE-D3(BJ) level of theory, where active sites were stabilized by the negative charges of framework Al T-sites located in the side pocket of mordenite.

The Cu-oxo species was represented by the $[Cu_3O_3]^{2+}$ trimeric cluster configuration determined with a recently developed expert bias-free computational procedure.[33] The structure of the Cu-Al-oxo cluster, on the other hand, has been constructed assuming a metal-oxo core with metal stoichiometry Cu/Al = 2:1 and an overall +2 charge, based on the stoichiometry of the Cu-EFAl interactions and the concentration of BAS exchanged with Cu.[31] Based on the higher thermodynamic stability obtained for a $[Cu_2AlO_4H]^{2+}$ cluster, we prefer this structure over the previously proposed $[Cu_2AlO_3]^{2+}$ cluster (see Section S4.4 and Figure S2 in the Supporting Information). To determine the most stable geometries of this cationic complex, an exhaustive configurational search was carried out using the combination of the low-mode molecular dynamics (LMMD) and machine-learning clustering algorithm k-medoids approach[33−35] (see S4.1. and S4.2 in the Supporting Information). The employed molecular dynamics procedure provides an enhancement in the configurational search by dragging the system along the low-frequency mode. Linking the results of the LMMD with the clustering algorithm allows us to efficiently analyze the trajectories by grouping them based on the similar structural features they possess. The results of this postprocessing analysis are depicted in Figure 4, where the extracted centers of the formed clusters are shown. As the geometries derived from the clustering of the trajectories have uncompensated forces acting on atoms, they have been optimized to local minima and their respective energies have been compared with respect to the most stable configuration identified. A general workflow of analyzing the LMMD trajectories simulated with two distinct $[Cu_2AlO_4H]^{2+}$ starting geometries is illustrated in Figure S1.

In all geometries in Figure 4, a $[Cu_2AlO_3]^{2+}$ core can be identified. We also observe a few similar structures displayed within a single clustering procedure (Figure S1). This can be justified by a relatively low value of the Silhouette score—the separation quality metrics—for a portion of trajectories causing an overlap of the clusters in Figures S1a.2 and S1b.2. Nevertheless, there is substantial structural diversity in the extracted isomers. Taking into account the similarities, we have displayed structures as colored groups featuring the same structural identity within the group.

Among the isomers identified (Figure 4), the most stable configuration (**a.**) consists of a $[Cu_2AlO_3]^{2+}$ core augmented by an additional bridging μ-OH ligand coordinated to Cu and Al centers featuring distorted tetrahedral environments. Additional distortion of the Cu coordination environment gives rise to a similar but 0.5 eV less stable configuration (**b.**). Structures (**c.**)−(**d.**) that are 0.7−0.8 eV less stable than (**a.**) feature trigonal coordination of the EFAl ion bearing a terminal OH− group. Structures (**e.**)−(**g.**) contain the OH ligand in the terminal coordination to the tetrahedral EFAl center, resulting in only slightly lower stability of the respective isomers compared to **a.** (ΔE = 0.1−0.3 eV). Our procedure also identified less stable configurations containing a terminal oxyl ligand (**h.**) and (**j.**), at the EFAl (ΔE = 1.3 eV) and Cu (ΔE = 0.6 eV), respectively. Our sampling results indicate substantial configurational flexibility of the extraframework clusters with the most stable structures all featuring the experimentally observed $[Cu_2AlO_3]^{2+}$ core—with geometrical

https://doi.org/10.1021/jacs.3c04328
J. Am. Chem. Soc. 2023, 145, 17710−17719

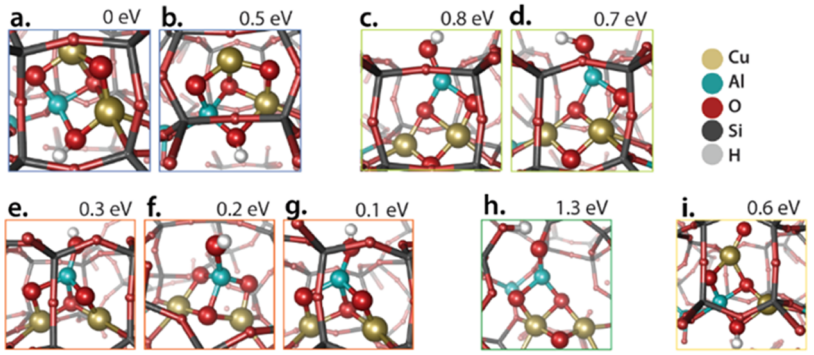

Figure 4. Centers of the clusters resulting from the k-medoids clustering of $[Cu_2AlO_4H]^{2+}$ LMMD trajectories analysis, grouped and colored based on their structural similarities: (a, b) $[Cu_2Al(\mu^3\text{-}O)(\mu^2\text{-}O)_2(\mu^2\text{-}OH)]^{2+}$, (c–g) $[Cu_2(\mu^3\text{-}O)(\mu^2\text{-}O)_2Al(OH)]^{2+}$, (h) $[Cu_2(\mu^3\text{-}O)(\mu^2\text{-}O)_2Al(O)]^{+}$,$H_Z^{+}$, and (i) $[(O)Cu_2(\mu^3\text{-}O)(\mu^2\text{-}O)(\mu^2\text{-}OH)Al]^{2+}$ coordinations. Relative stabilities of the extracted configurations with respect to the lowest-lying $[Cu_2Al(\mu^3\text{-}O)(\mu^2\text{-}O)_2(\mu^2\text{-}OH)]^{2+}$ state presented in (a) are given in eV.

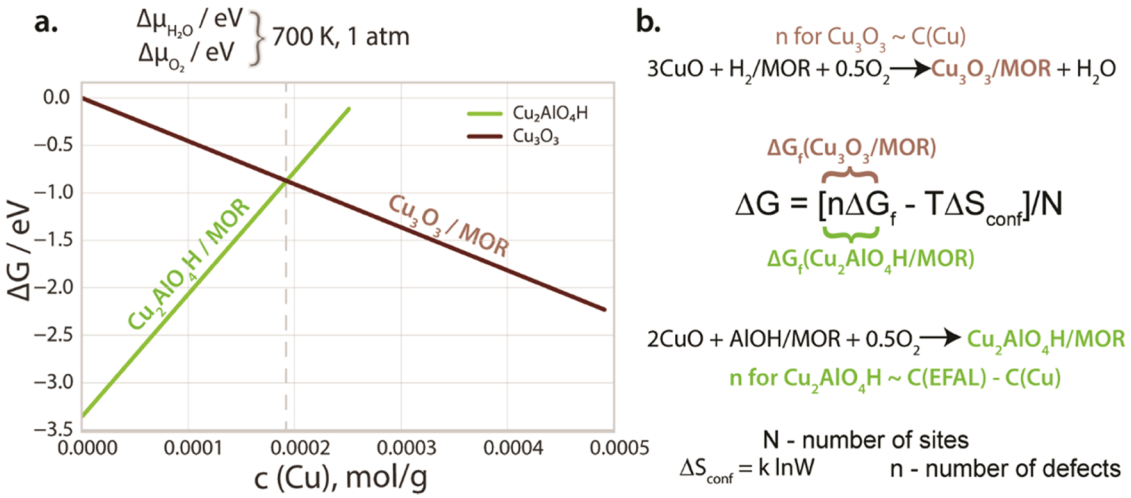

Figure 5. (a) Thermodynamic stability of the $[Cu_2AlO_4H]^{2+}$ and $[Cu_3O_3]^{2+}$ complexes in EFAl-containing MOR zeolite model as a function of Cu contents computed under reactive conditions of 700 K and 1 atm. (b) Defect model approximation and accounting for concentration dependencies and configurational entropy terms.

features similar to those identified by EXAFS[31] (see Figure S7 in the Supporting Information)—and different positions for the OH ligand. Hirshfeld charge analysis reveals that similar to that in pure Cu-oxo $[Cu_3O_3]^{2+}$ species,[18] all Cu ions in $[Cu_2AlO_4H]^{2+}$ complexes are in +2 formal oxidation state, while two of the three extraframework oxygens have a pronounced radical character (Table S6, Figure S4).

To theoretically describe the experimentally observed change in the Cu-oxo and Cu-Al-oxo speciation as a function of Cu concentration (Figure 3), a new thermodynamic model has been developed and integrated within the aiTA framework. In this approach, we take as reference states the ideal H-form of the zeolite and the relevant stable metal oxide (CuO in this case). Such reference states are condition-independent, allowing for an unbiased thermodynamic analysis of the stability of different extraframework species in the zeolite pores. This reference state has earlier successfully been used for the analysis of different Cu species.[16,36] In this work, we propose to treat the extraframework (EF) cations as defects in the zeolite matrix.[37] The Gibbs free energy change for the formation of an EF ensemble with a given stoichiometry includes the intrinsic free energy of the formation of a single EF species, the concentration of the EF species, as well as the associated configurational entropy terms (eq E8 in S4.5 in the Supporting Information). Here, we consider the formation of the Cu-oxo or Cu-Al-oxo cationic complexes as "defects" in a MOR material with a given concentration of isolated EFAl species and BAS, at conditions similar to the activation of Cu-zeolite materials: 1 bar and 700 K.

The reaction of CuO as the reference copper source with either the BAS or EFAl species yields Cu-oxo or Cu-Al-oxo complexes, respectively. For the Cu-oxo extraframework species, the number of defects is proportional to the experimental concentration of Cu defined in a range of [0; 500] μmol/g, whereas the number of defects of the Cu-Al-oxo species depends on both the concentration of the EFAl species and Cu. The concentration of the EFAl species in the parent MOR material was experimentally set as 260 μmol/g, according to ^{27}Al MAS NMR and the IR spectra of adsorbed pyridine.[31] The key approximations for the concentration-dependent standard Gibbs free energy expressions for the $[Cu_3O_3]^{2+}$ and $[Cu_2AlO_4H]^{2+}$ defects (eq E12 and E13) are explained in detail in S4.5 based on earlier computational studies.[37,38]

Figure 5 compares the stability of the bimetallic $[Cu_2AlO_4H]^{2+}$ species and the separate $[Cu_3O_3]^{2+}$ and EFAl as a function of Cu contents in a model MOR zeolite. The thermodynamic analysis shows that, at low loadings, copper

https://doi.org/10.1021/jacs.3c04328
J. Am. Chem. Soc. 2023, 145, 17710−17719

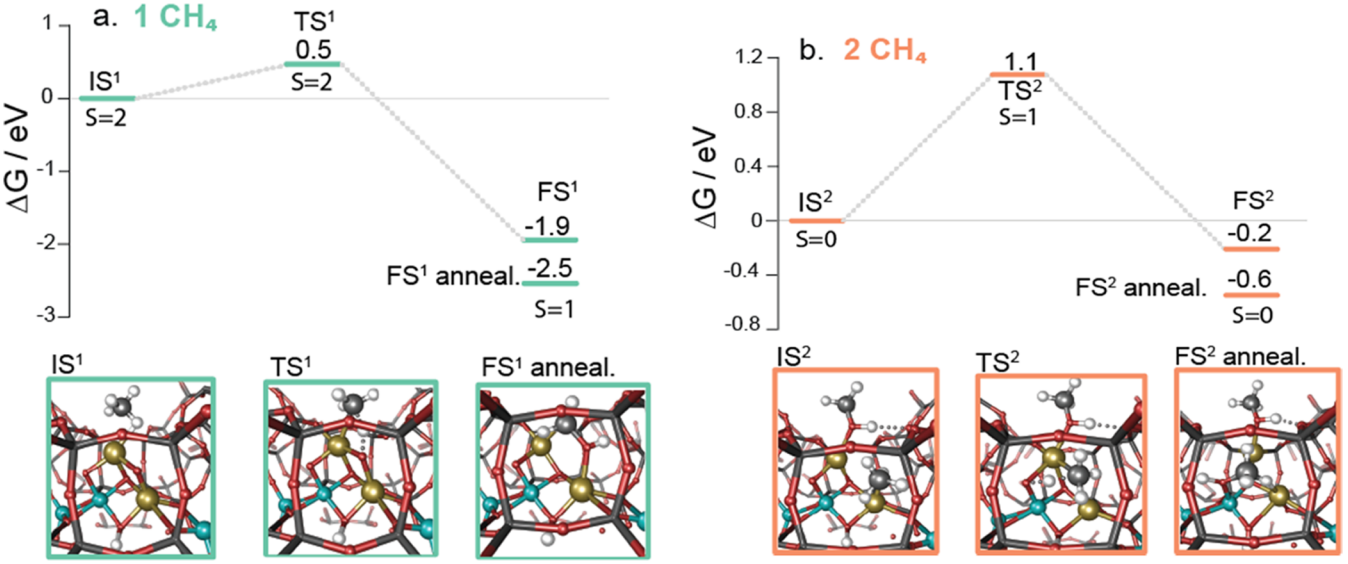

Figure 6. Reaction energy diagrams for (a) the first and (b) second methane molecule oxidation by the $[Cu_2AlO_4H]^{2+}$ cation in MOR. Spin states are indicated. The annealing procedure revealed the possibility of an additional stabilization of the surface oxidation products (FS → FS_{anneal}) via a facile isomerization process. The final states undergo the procedure of annealing to converge to the near-lying energy basin on the potential energy surface.

preferentially binds with the EFAl sites to form the bimetallic species. However, with increasing Cu contents, the separation of the cationic EFAl and Cu species becomes thermodynamically more favorable. Our model predicts that for overall Cu concentrations of ca. 200 μmol/g, the formation of Cu_3O_3 cluster is preferred over the formation of Cu_2AlO_4H, in excellent agreement with the experimental results (Figure 3). Note, however, that this might be coincidental because the standard free energies computed in the presented scheme depend on the choice of the EFAl structure and the initial assumption of the zeolite composition (BAS and EFAl concentration). In practice, the formation of clusters occurs during the thermal treatment in oxidative conditions after ion exchange, after the removal of H_2O coordinating Cu ions.[23,39] In that process, it will be the concentration of Cu and EFAl ions near preferred exchange sites—which are known to be the 8 MR sites in MOR[40]—the factor determining the formation of a Cu-oxo or a Cu-Al-oxo cluster. Based on our thermodynamic calculations, at sufficiently high concentrations of Cu, the Cu-oxo cluster will be preferred.

Next, periodic DFT calculations were carried out to evaluate the reactivity of the most stable $[Cu_2AlO_4H]^{2+}$ in MOR toward the activation of multiple methane molecules. Figure 6 presents the computed reaction energy diagrams for the sequential methane activation by the bimetallic cation. In both steps, C−H bond activation follows a homolytic radical reaction followed by a facile rebound to form CH_3OH (1st CH_4 activation, FS^1) or CH_3O- and OH− species (2nd CH_4 activation, FS^2) adsorbed to the cationic cluster. An additional annealing procedure on the reaction intermediate formed via the elementary C−H activation processes showed that a facile isomerization leads to an additional stabilization of the surface intermediates by 0.4−0.6 eV. Both steps proceed with relatively low activation barriers. The oxidation of the first CH_4 molecule proceeds with a barrier of about 0.5 eV, whereas the subsequent C−H activation by the thus formed partially reduced dual-metal cation faces a much higher barrier of 1.1 eV. The values of the single imaginary frequencies along the reaction paths are listed in Table S5.

To further assess the thermodynamics of methane activation under the experimentally relevant conditions, an *ab initio* thermodynamic analysis has been carried out, and the results are presented in Figure 7 (the computational details and the model definitions are summarized in Section S4.6 in the Supporting information). For comparison, a similar analysis has been carried out for pure $[Cu_3O_3]^{2+}$ (see Section S4.6 for details). The computations show that the hydroxylated $[Cu_2AlO_4H]^{2+}$ cluster proposed here, despite its high intrinsic

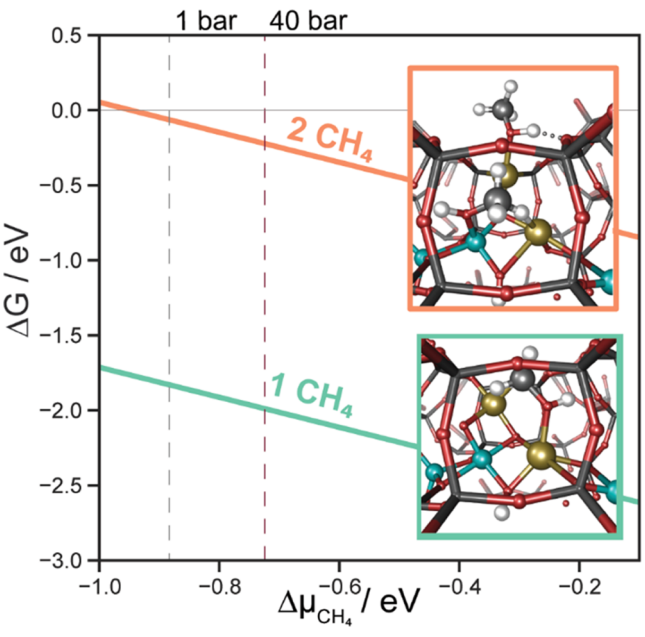

Figure 7. Computed Gibbs free energies of sequential activation of methane by $[Cu_2AlO_4H]^{2+}$ active site situated in the side pocket of mordenite as a function of $\Delta\mu_{CH4}$. The geometries of the corresponding intermediate surface products are displayed.

https://doi.org/10.1021/jacs.3c04328
J. Am. Chem. Soc. 2023, 145, 17710−17719

thermodynamic stability, is capable of oxidizing up to two methane molecules per complex under ambient pressure. On the contrary, the activation of the second methane molecule by the pure Cu-oxo species $[Cu_3O_3]^{2+}$ is only feasible at elevated pressures (Figure S3).

Based on aiTA calculations, $[Cu_3O_3]^{2+}$ clusters activate 1 CH_4 molecule at 1 bar and 2 CH_4 molecules at 40 bar,[17] while $[Cu_2AlO_4H]^{2+}$ clusters activate 2 CH_4 molecules at pressures ≥1 bar (Figure 5a). By using the concentrations of $[Cu_2AlO_4H]^{2+}$ and $[Cu_3O_3]^{2+}$ clusters as determined from activity tests at 1 bar (Figure 3), we show that this model predicts well the activity at 40 bar of EFAl-containing Cu-MOR samples with different Cu loadings (Figure 8a).

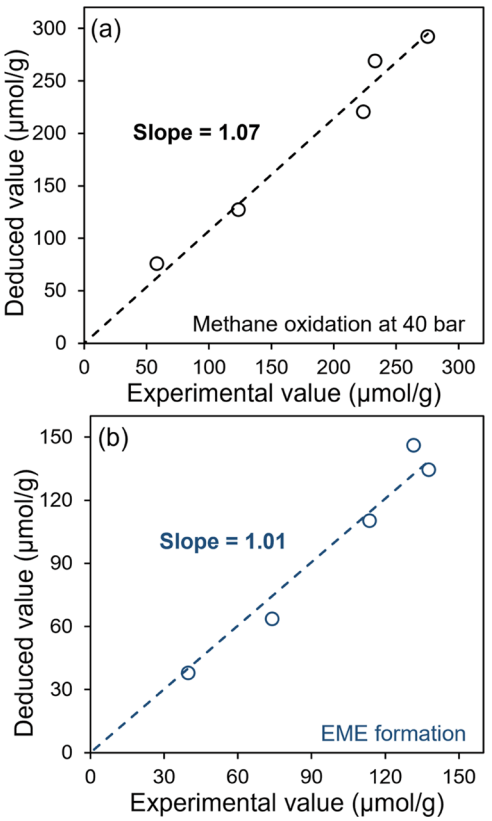

Figure 8. (a) Correlation of the methanol yields achieved at 40 bar and the deduced value from the cluster distribution; (b) correlation of the EME yields achieved at 1 bar and the deduced value from the cluster distribution.

Likewise, we have observed that, in the case of Cu-MOR materials with low Cu loading, the ethanol post-treatment extracted less CH_3- than the treatment with H_2O (Figure 2). According to our model, at low loadings, a majority of Cu-Al-oxo clusters are expected to be present in the material. The experimental data in this study show the higher stability and lower reactivity of the CH_3 moieties formed on the Cu-Al-oxo clusters than on pure Cu-oxo under the ethanol treatment applied here, and only a fraction of the activated methyl species reacts further to gas products. We speculate that this lower reactivity is related to the higher stability of the structure of the spent Cu-Al-oxo cluster. Overall, and based on our data, both structures are expected to form one EME molecule per cluster after reaction at 1 bar. Based on this assumption, we have calculated the EME yields expected for each Cu-MOR sample, given the concentration of each type of cluster (Table S2 and Figure 3). In Figure 8b, it can be seen that the calculated EME yields correlate very well with the experimental data. These results show that the two-cluster model agrees well with the activity performances in various conditions.

The lack of reactivity with ethanol of the second CH_4 molecule on the $[Cu_2AlO_4H]^{2+}$ cluster is tentatively attributed to the local constraints resulting from the bulky transition state during the ether formation process in the MOR pore structure.

Spectroscopic Evidences on the Cluster Distributions. The identification of active Cu-oxo structures using spectroscopies has emerged as a particularly challenging task. In spite of the enormous potential of X-ray absorption to identify small-size structures, experimental and theoretical analysis have led to conflicting results, often as a result of large contributions or interferences of inactive Cu species to the spectral task.[41] Therefore, we address here the characterization of Cu-MOR materials containing virtually only active Cu species[31] with a set of different and complementary spectroscopies. The spectra reveal features that either confirm or rule out structural proposals. Such proposals are based on theory calculations and the CH_4-to-metal (and CH_4-to-oxo) stoichiometries obtained from methane oxidation tests.

First, we examined the differences observed in the Cu L_3-edge X-ray absorption near-edge structure (XANES) of O_2-activated Cu-MOR samples with different Cu loadings. The main peak at 929 eV corresponds to 2p to 3d dipole transitions of Cu(II) species. The position of the satellite feature that arises from the mixing of Cu 3d orbitals with 2p orbitals from the oxygen ligands generally reveals information on the local chemical environment of the Cu species hosted in each material.[42,43] While the materials containing 160 and 280 μmol/g of Cu both show a satellite peak at ΔE = 3.5 eV, the satellite feature for the sample with ca. 450 μmol/g of Cu appears at ΔE = 3.2 eV (Figure 9). In our previous work, the satellite peak for the simulated spectra of $[Cu_2AlO_3]^{2+}$ homologue appears at ΔE 3.3 eV, while the satellite feature for $[Cu_3O_3]^{2+}$ cluster shows up at ca. ΔE 2.0 eV.[31] Therefore, we propose that the shift toward lower energies of the satellite

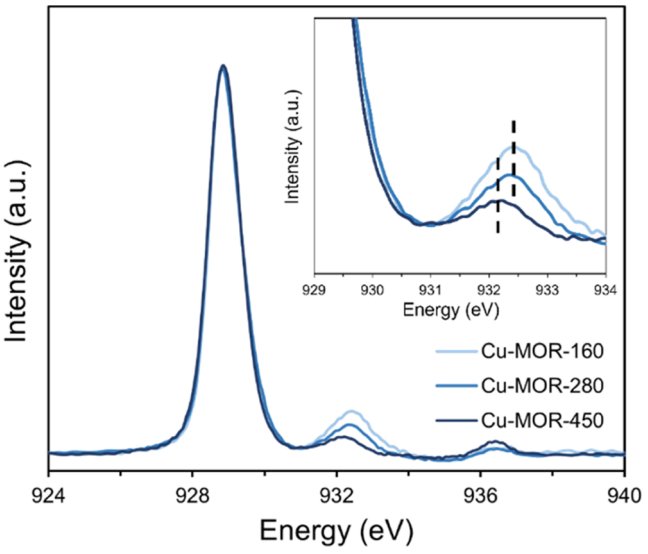

Figure 9. Cu L_3-edge XANES of Cu-MOR samples activated in O_2 at 450 °C for 1 h. Spectra normalized to the intensities of the main edge for the sake of visualization of the satellite position.

https://doi.org/10.1021/jacs.3c04328
J. Am. Chem. Soc. 2023, 145, 17710−17719

peak with increasing Cu loading is indicative of a larger contribution of $[Cu_3O_3]^{2+}$ clusters, in good agreement with the relative concentrations calculated in Figure 3.

The EFAl-containing Cu-MOR samples after CH_4 exposure were investigated by in situ UV−vis spectroscopy. The difference spectra, obtained by subtracting the spectra after CH_4 exposure for 30 min from those of the oxygen-activated samples, show decreasing absorption bands at 29 000 and 39 000 cm^{-1} (Figures 10a and S5 and S6), which have been

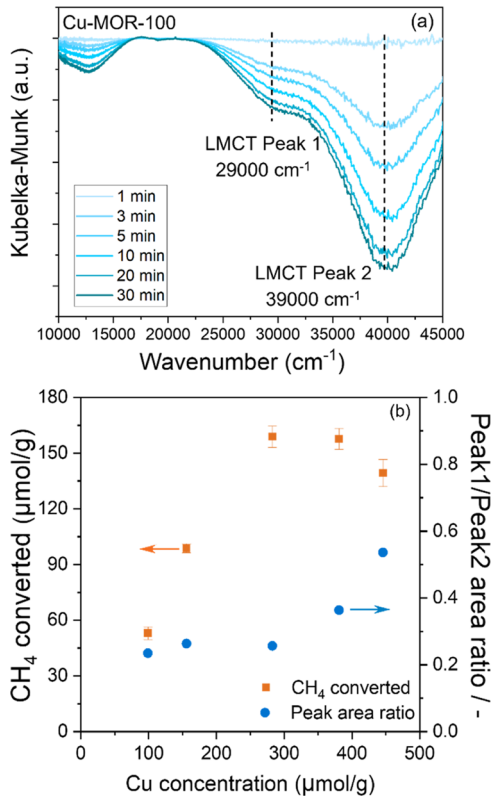

Figure 10. (a) In situ UV−vis difference spectra of an oxygen activated Cu-MOR containing 100 μmol/g Cu, after exposure to CH_4 at 200 °C for 30 min. (b) Peak area ratio of the decrease of two LMCT bands from UV−vis absorption spectra upon activation of methane at 1 bar as a function of Cu concentration in MOR (see UV−vis spectra of all Cu-MOR materials in Section S5).

attributed in literature to the intensity change of the charge transfer bands of extraframework[11,16,44] and framework oxygen atoms,[45,46] respectively, to Cu species during CH_4 reaction. Note also the appearance of an adsorption band at 18 000 cm^{-1} that becomes increasingly intense for Cu-MOR samples with high Cu loadings (Figure S5) and that we tentatively attribute to the d−d transition of Cu(II) species formed upon reaction with CH_4. The presence of Cu(II) in the spent Cu-oxo clusters can be expected for the case in which only one CH_4 molecule is activated per cluster (see Supporting Information Table S7), which is, as described here, the stoichiometry of CH_4 activation at atmospheric pressure over $[Cu_3O_3]^{2+}$. The relative ratios of the two Cu-oxo-related features at 29 000 and 39 000 cm^{-1} stay roughly between 0.2 and 0.3 for samples with Cu concentrations lower than 300 μmol/g, while they gradually increase up to 0.54 at higher Cu loadings (see Section S5 in the SI and Figure S5 therein). It should be noted that ratios of ca. 0.5 have been observed for conventional Cu-MOR sample containing solely $[Cu_3O_3]^{2+}$ clusters (Figure S5f). The concentration of extraframework oxygens directly bound to Cu in the $[Cu_3O_3]^{2+}$ cluster is higher than that in $[Cu_2AlO_4H]^{2+}$ clusters and, therefore, the Peak 1/Peak 2 ratio as in Figure 10 is expected to increase with the relative concentration of $[Cu_3O_3]^{2+}$. Based on this, we attribute the decrease of the band at ca. 39 000 cm^{-1} upon CH_4 loading to the activation of CH_4 on μ-oxo bridges present on both Cu-oxo and Cu-Al oxo clusters. Conversely, the 29 000 cm^{-1} band decrease is a fingerprint of CH_4 activation over monometallic Cu-oxo clusters, namely, Cu−O−Cu bridges in $[Cu_3O_3]^{2+}$ clusters, as previously reported.[16] Therefore, the changes in the relative contribution of each UV−vis band agree well with the present structural proposal of Cu-oxo and Cu-Al-oxo clusters, and they are qualitatively consistent with the expected concentrations of each type of cluster for Cu-MOR materials with different Cu loadings (Figure 3).

CONCLUSIONS

A series of highly active Cu-MOR samples containing EFAl were synthesized and investigated for selective CH_4 oxidation at ambient and elevated CH_4 pressure. These materials have significantly higher yields to methanol than previously reported materials. This is attributed to the formation of Cu-Al-oxo species that are more efficient than their Cu-oxo counterparts. Their synthetic potential has been expanded further to the preparation of ethyl methyl ether by replacing H_2O with ethanol in the extraction step. The aiTA combined with MD calculations allowed us to identify the stoichiometry and geometry of the active Cu-Al-oxo clusters as a Cu_2AlO_3 structural core with an OH ligand. Contrary to the previously described $[Cu_3O_3]^{2+}$ cluster, this $[Cu_2AlO_4H]^{2+}$ cluster can readily activate two CH_4 molecules per cluster at 200 °C and 1 bar CH_4. A thermodynamic equilibrium has been found between the formation of $[Cu_2AlO_4H]^{2+}$ and $[Cu_3O_3]^{2+}$ clusters as a function of the Cu concentration in MOR during the ion exchange. Based on the CH_4 oxidation activity at different pressures, we have calculated the concentration of each type of Cu-(Al-)oxo cluster formed in MOR. Spectroscopic characterization supported the presence of the two clusters and the change in relative proportions with Cu loading.

Based on the observations reported here, we conclude that, in the synthesis of highly active catalysts based on Cu and other metal ion-exchanged zeolites, it should be considered the competition between different metal-oxo cluster structures and stoichiometries within the available metal ion concentrations, together with the thermodynamic stability of the clusters at the reaction conditions.

The positive impact of EFAl on the activity of Cu-MOR has been described quantitatively, aiding the synthesis of novel Cu-based catalysts with highly active and selective oxygen species for the conversion of light alkanes. The understanding of the speciation of Cu ions and oxo clusters in zeolites has enabled the geometric description of active structures, and the results shed light on metal-oxo ensembles capable of stabilizing oxygen species with exceptional catalytic properties.

ASSOCIATED CONTENT

Supporting Information

The Supporting Information is available free of charge at https://pubs.acs.org/doi/10.1021/jacs.3c04328.

https://doi.org/10.1021/jacs.3c04328
J. Am. Chem. Soc. 2023, 145, 17710−17719

Materials and experimental methods (S1); chemical composition and degree of exchange of Cu-MOR samples (S2); calculation of concentrations of Cu-oxo and Cu-Al-oxo clusters as in Figure 3b (S3); supplementary computational details (S4); in situ UV−vis spectroscopy (S5); and supplementary references (S6) (PDF)

Optimized structures in the .xyz format (Data_SI) (ZIP)

AUTHOR INFORMATION

Corresponding Authors

Evgeny A. Pidko − *Inorganic Systems Engineering (ISE), Department of Chemical Engineering, Delft University of Technology, 2629 HZ Delft, The Netherlands;* orcid.org/0000-0001-9242-9901; Email: e.a.pidko@tudelft.nl

Maricruz Sanchez-Sanchez − *Department of Chemistry and Catalysis Research Center, Technische Universität München, 85748 Garching, Germany; Institute of Chemical, Environmental and Bioscience Engineering, TU Wien, 1060 Vienna, Austria;* orcid.org/0000-0002-3769-9623; Email: maricruz.sanchez@tuwien.ac.at

Johannes A. Lercher − *Department of Chemistry and Catalysis Research Center, Technische Universität München, 85748 Garching, Germany; Institute for Integrated Catalysis, Pacific Northwest National Laboratory, Richland, Washington 99352, United States;* orcid.org/0000-0002-2495-1404; Email: johannes.lercher@ch.tum.de

Authors

Lei Tao − *Department of Chemistry and Catalysis Research Center, Technische Universität München, 85748 Garching, Germany*

Elena Khramenkova − *Inorganic Systems Engineering (ISE), Department of Chemical Engineering, Delft University of Technology, 2629 HZ Delft, The Netherlands*

Insu Lee − *Department of Chemistry and Catalysis Research Center, Technische Universität München, 85748 Garching, Germany*

Takaaki Ikuno − *Department of Chemistry and Catalysis Research Center, Technische Universität München, 85748 Garching, Germany*

Rachit Khare − *Department of Chemistry and Catalysis Research Center, Technische Universität München, 85748 Garching, Germany;* orcid.org/0000-0002-1519-5184

Andreas Jentys − *Department of Chemistry and Catalysis Research Center, Technische Universität München, 85748 Garching, Germany*

John L. Fulton − *Institute for Integrated Catalysis, Pacific Northwest National Laboratory, Richland, Washington 99352, United States;* orcid.org/0000-0001-9361-9803

Alexander A. Kolganov − *Inorganic Systems Engineering (ISE), Department of Chemical Engineering, Delft University of Technology, 2629 HZ Delft, The Netherlands;* orcid.org/0000-0002-0262-8892

Complete contact information is available at: https://pubs.acs.org/10.1021/jacs.3c04328

Author Contributions

[⊥]L.T. and E.K. contributed equally to this work.

Notes

The authors declare no competing financial interest.

ACKNOWLEDGMENTS

This article is adapted from part of the PhD Thesis of L.Tao *Formation of Cu-Al-Oxo clusters in zeolites for selective oxidation of methane to methanol*, TU Munich, 2022, and part of the PhD Thesis of E.V. Khramenkova *Mapping the reaction landscape for the C1 chemistry*, Delft University of Technology, 2022. The financial support from the Deutsche Forschungsgemeinschaft (DFG, Project Number 326562156) and the TUM International Graduate School of Science and Engineering (IGSSE) is acknowledged. J.A.L. and J.L.F. acknowledge the support by the U.S. Department of Energy (DOE), Office of Science, Office of Basic Energy Sciences (BES), Division of Chemical Sciences, Geosciences and Biosciences (Impact of catalytically active centers and their environment on rates and thermodynamic states along reaction paths, FWP 47319). E.A.P. acknowledges financial support from the European Research Council (ERC) under the European Union's Horizon 2020 research and innovation programme (grant agreement no. 725686). The use of supercomputer facilities was sponsored by NWO Domain Science. The ensemble explorations were carried out using the DECI resource Tetralith of the National Supercomputer Centre at Linköping University with support from the PRACE (DECI 17). The authors are thankful to the Paul Scherrer Institut, Villigen, Switzerland, for the provision of synchrotron beamtime at beamline PHOENIX of the SLS.

REFERENCES

(1) Malakoff, D. The gas surge. *Science* **2014**, *344*, 1464.

(2) Kerr, R. A. Natural Gas From Shale Bursts Onto the Scene. *Science* **2010**, *328*, 1624.

(3) Caballero, A.; Perez, P. J. Methane as raw material in synthetic chemistry: the final frontier. *Chem. Soc. Rev.* **2013**, *42*, 8809−8820.

(4) Periana, R. A.; Taube, D. J.; Gamble, S.; Taube, H.; Satoh, T.; Fujii, H. Platinum Catalysts for the High-Yield Oxidation of Methane to a Methanol Derivative. *Science* **1998**, *280*, 560.

(5) Schwarz, H. Chemistry with Methane: Concepts Rather than Recipes. *Angew. Chem., Int. Ed.* **2011**, *50*, 10096−10115.

(6) Rosenzweig, A. C. Particulate Methane Monooxygenase. In *Handbook of Metalloproteins*; John Wiley & Sons, Ltd., 2004.

(7) Ross, M. O.; Rosenzweig, A. C. A tale of two methane monooxygenases. *JBIC, J. Biol. Inorg. Chem.* **2017**, *22*, 307−319.

(8) Sazinsky, M. H.; Lippard, S. J. Methane Monooxygenase: Functionalizing Methane at Iron and Copper. In *Sustaining Life on Planet Earth: Metalloenzymes Mastering Dioxygen and Other Chewy Gases*; Kroneck, P. M. H.; Sosa Torres, M. E., Eds.; Springer International Publishing: Cham, 2015; pp 205−256.

(9) Solomon, E. I.; Heppner, D. E.; Johnston, E. M.; Ginsbach, J. W.; Cirera, J.; Qayyum, M.; Kieber-Emmons, M. T.; Kjaergaard, C. H.; Hadt, R. G.; Tian, L. Copper Active Sites in Biology. *Chem. Rev.* **2014**, *114*, 3659−3853.

(10) Mahyuddin, M. H.; Tanaka, T.; Shiota, Y.; Staykov, A.; Yoshizawa, K. Methane Partial Oxidation over $[Cu_2(\mu\text{-}O)]^{2+}$ and $[Cu_3(\mu\text{-}O)_3]^{2+}$ Active Species in Large-Pore Zeolites. *ACS Catal.* **2018**, *8*, 1500−1509.

(11) Le, H. V.; Parishan, S.; Sagaltchik, A.; Göbel, C.; Schlesiger, C.; Malzer, W.; Trunschke, A.; Schomäcker, R.; Thomas, A. Solid-State Ion-Exchanged Cu/Mordenite Catalysts for the Direct Conversion of Methane to Methanol. *ACS Catal.* **2017**, *7*, 1403−1412.

(12) Snyder, B. E. R.; Vanelderen, P.; Schoonheydt, R. A.; Sels, B. F.; Solomon, E. I. Second-Sphere Effects on Methane Hydroxylation in Cu-Zeolites. *J. Am. Chem. Soc.* **2018**, *140*, 9236−9243.

(13) Brezicki, G.; Kammert, J. D.; Gunnoe, T. B.; Paolucci, C.; Davis, R. J. Insights into the Speciation of Cu in the Cu-H-Mordenite Catalyst for the Oxidation of Methane to Methanol. *ACS Catal.* **2019**, *9*, 5308−5319.

(14) Pappas, D. K.; Martini, A.; Dyballa, M.; Kvande, K.; Teketel, S.; Lomachenko, K. A.; Baran, R.; Glatzel, P.; Arstad, B.; Berlier, G.; Lamberti, C.; Bordiga, S.; Olsbye, U.; Svelle, S.; Beato, P.; Borfecchia, E. The Nuclearity of the Active Site for Methane to Methanol Conversion in Cu-Mordenite: A Quantitative Assessment. *J. Am. Chem. Soc.* **2018**, *140*, 15270−15278.
(15) Grundner, S.; Luo, W.; Sanchez-Sanchez, M.; Lercher, J. A. Synthesis of single-site copper catalysts for methane partial oxidation. *Chem. Commun.* **2016**, *52*, 2553−2556.
(16) Grundner, S.; Markovits, M. A. C.; Li, G.; Tromp, M.; Pidko, E. A.; Hensen, E. J. M.; Jentys, A.; Sanchez-Sanchez, M.; Lercher, J. A. Single-site trinuclear copper oxygen clusters in mordenite for selective conversion of methane to methanol. *Nat. Commun.* **2015**, *6*, No. 7546.
(17) Zheng, J.; Lee, I.; Khramenkova, E.; Wang, M.; Peng, B.; Gutiérrez, O. Y.; Fulton, J. L.; Camaioni, D. M.; Khare, R.; Jentys, A.; Haller, G. L.; Pidko, E. A.; Sanchez-Sanchez, M.; Lercher, J. A. Importance of methane chemical potential for its conversion to methanol on Cu-exchanged mordenite. *Chem. − Eur. J.* **2020**, *26*, 7563−7567.
(18) Vogiatzis, K. D.; Li, G.; Hensen, E. J. M.; Gagliardi, L.; Pidko, E. A. Electronic Structure of the $[Cu_3(\mu\text{-}O)_3]^{2+}$ Cluster in Mordenite Zeolite and Its Effects on the Methane to Methanol Oxidation. *J. Phys. Chem. C* **2017**, *121*, 22295−22302.
(19) Dandu, N. K.; Reed, J. A.; Odoh, S. O. Performance of Density Functional Theory for Predicting Methane-to-Methanol Conversion by a Tri-Copper Complex. *J. Phys. Chem. C* **2018**, *122*, 1024−1036.
(20) Sushkevich, V. L.; Palagin, D.; Ranocchiari, M.; van Bokhoven, J. A. Selective anaerobic oxidation of methane enables direct synthesis of methanol. *Science* **2017**, *356*, 523.
(21) Sushkevich, V. L.; van Bokhoven, J. A. Effect of Brønsted acid sites on the direct conversion of methane into methanol over copper-exchanged mordenite. *Catal. Sci. Technol.* **2018**, *8*, 4141−4150.
(22) Markovits, M. A. C.; Jentys, A.; Tromp, M.; Sanchez-Sanchez, M.; Lercher, J. A. Effect of Location and Distribution of Al Sites in ZSM-5 on the Formation of Cu-Oxo Clusters Active for Direct Conversion of Methane to Methanol. *Top. Catal.* **2016**, *59*, 1554−1563.
(23) Pappas, D. K.; Borfecchia, E.; Dyballa, M.; Pankin, I. A.; Lomachenko, K. A.; Martini, A.; Signorile, M.; Teketel, S.; Arstad, B.; Berlier, G.; Lamberti, C.; Bordiga, S.; Olsbye, U.; Lillerud, K. P.; Svelle, S.; Beato, P. Methane to Methanol: Structure-Activity Relationships for Cu-CHA. *J. Am. Chem. Soc.* **2017**, *139*, 14961−14975.
(24) Dyballa, M.; Pappas, D. K.; Kvande, K.; Borfecchia, E.; Arstad, B.; Beato, P.; Olsbye, U.; Svelle, S. On How Copper Mordenite Properties Govern the Framework Stability and Activity in the Methane-to-Methanol Conversion. *ACS Catal.* **2019**, *9*, 365−375.
(25) Tao, L.; Lee, I.; Sanchez-Sanchez, M. Cu oxo nanoclusters for direct oxidation of methane to methanol: formation, structure and catalytic performance. *Catal. Sci. Technol.* **2020**, *10*, 7124−7141.
(26) Mahyuddin, M. H.; Staykov, A.; Shiota, Y.; Miyanishi, M.; Yoshizawa, K. Roles of Zeolite Confinement and Cu−O−Cu Angle on the Direct Conversion of Methane to Methanol by $[Cu_2(\mu\text{-}O)]^{2+}$-Exchanged AEI, CHA, AFX, and MFI Zeolites. *ACS Catal.* **2017**, *7*, 3741−3751.
(27) Newton, M. A.; Knorpp, A. J.; Sushkevich, V. L.; Palagin, D.; van Bokhoven, J. A. Active sites and mechanisms in the direct conversion of methane to methanol using Cu in zeolitic hosts: a critical examination. *Chem. Soc. Rev.* **2020**, *49*, 1449−1486.
(28) Tao, L.; Lee, I.; Khare, R.; Jentys, A.; Fulton, J. L.; Sanchez-Sanchez, M.; Lercher, J. A. Speciation of Cu-Oxo Clusters in Ferrierite for Selective Oxidation of Methane to Methanol. *Chem. Mater.* **2022**, *34*, 4355−4363.
(29) Mohan, S.; Dinesha, P.; Kumar, S. NOx reduction behaviour in copper zeolite catalysts for ammonia SCR systems: A review. *Chem. Eng. J.* **2020**, *384*, No. 123253.
(30) Han, L.; Cai, S.; Gao, M.; Hasegawa, J.-y.; Wang, P.; Zhang, J.; Shi, L.; Zhang, D. Selective Catalytic Reduction of NOx with NH_3 by Using Novel Catalysts: State of the Art and Future Prospects. *Chem. Rev.* **2019**, *119*, 10916−10976.
(31) Lee, I.; Lee, M.-S.; Tao, L.; Ikuno, T.; Khare, R.; Jentys, A.; Huthwelker, T.; Borca, C. N.; Kalinko, A.; Gutiérrez, O. Y.; Govind, N.; Fulton, J. L.; Hu, J. Z.; Glezakou, V.-A.; Rousseau, R.; Sanchez-Sanchez, M.; Lercher, J. A. Activity of Cu−Al−Oxo Extra-Framework Clusters for Selective Methane Oxidation on Cu-Exchanged Zeolites. *JACS Au* **2021**, *1*, 1412−1421.
(32) Tomkins, P.; Mansouri, A.; Bozbag, S. E.; Krumeich, F.; Park, M. B.; Alayon, E. M.; Ranocchiari, M.; van Bokhoven, J. A. Isothermal Cyclic Conversion of Methane into Methanol over Copper-Exchanged Zeolite at Low Temperature. *Angew. Chem., Int. Ed.* **2016**, *55*, 5467−5471.
(33) Khramenkova, E. V.; Medvedev, M. G.; Li, G.; Pidko, E. A. Unraveling the Nature of Extraframework Catalytic Ensembles in Zeolites: Flexibility and Dynamics of the Copper-Oxo Trimers in Mordenite. *J. Phys. Chem. Lett.* **2021**, *12*, 10906−10913.
(34) Medvedev, M. G.; Panova, M. V.; Chilov, G. G.; Bushmarinov, I. S.; Novikov, F. N.; Stroganov, O. V.; Zeifman, A. A.; Svitanko, I. V. Exhaustive conformational search for transition states: the case of catechol O-methyltransferase active site. *Mendeleev Commun.* **2017**, *27*, 224−227.
(35) Medvedev, M. G.; Zeifman, A. A.; Novikov, F. N.; Bushmarinov, I. S.; Stroganov, O. V.; Titov, I. Y.; Chilov, G. G.; Svitanko, I. V. Quantifying Possible Routes for SpnF-Catalyzed Formal Diels−Alder Cycloaddition. *J. Am. Chem. Soc.* **2017**, *139*, 3942−3945.
(36) Li, G.; Vassilev, P.; Sanchez-Sanchez, M.; Lercher, J. A.; Hensen, E. J. M.; Pidko, E. A. Stability and reactivity of copper oxo-clusters in ZSM-5 zeolite for selective methane oxidation to methanol. *J. Catal.* **2016**, *338*, 305−312.
(37) Sutton, C.; Levchenko, S. V. First-Principles Atomistic Thermodynamics and Configurational Entropy. *Front. Chem.* **2020**, *8*, 757.
(38) Zhang, X.; Grabowski, B.; Hickel, T.; Neugebauer, J. Calculating free energies of point defects from ab initio. *Comput. Mater. Sci.* **2018**, *148*, 249−259.
(39) Ikuno, T.; Grundner, S.; Jentys, A.; Li, G.; Pidko, E.; Fulton, J.; Sanchez-Sanchez, M.; Lercher, J. A. Formation of Active Cu-oxo Clusters for Methane Oxidation in Cu-Exchanged Mordenite. *J. Phys. Chem. C* **2019**, *123*, 8759−8769.
(40) Veefkind, V. A.; Smidt, M. L.; Lercher, J. A. On the role of strength and location of Brønsted acid sites for ethylamine synthesis on mordenite catalysts. *Appl. Catal., A* **2000**, *194-195*, 319−332.
(41) Newton, M. A.; Knorpp, A. J.; Meyet, J.; Stoian, D.; Nachtegaal, M.; Clark, A. H.; Safonova, O. V.; Emerich, H.; van Beek, W.; Sushkevich, V. L.; van Bokhoven, J. A. Unwanted effects of X-rays in surface grafted copper(ii) organometallics and copper exchanged zeolites, how they manifest, and what can be done about them. *Phys. Chem. Chem. Phys.* **2020**, *22*, 6826−6837.
(42) Qayyum, M. F.; Sarangi, R.; Fujisawa, K.; Stack, T. D. P.; Karlin, K. D.; Hodgson, K. O.; Hedman, B.; Solomon, E. I. L-Edge X-ray Absorption Spectroscopy and DFT Calculations on Cu_2O_2 Species: Direct Electrophilic Aromatic Attack by Side-on Peroxo Bridged Dicopper(II) Complexes. *J. Am. Chem. Soc.* **2013**, *135*, 17417−17431.
(43) Sarangi, R.; Aboelella, N.; Fujisawa, K.; Tolman, W. B.; Hedman, B.; Hodgson, K. O.; Solomon, E. I. X-ray Absorption Edge Spectroscopy and Computational Studies on $LCuO_2$ Species: Superoxide−CuII versus Peroxide−CuIII Bonding. *J. Am. Chem. Soc.* **2006**, *128*, 8286−8296.
(44) Wulfers, M. J.; Teketel, S.; Ipek, B.; Lobo, R. F. Conversion of methane to methanol on copper-containing small-pore zeolites and zeotypes. *Chem. Commun.* **2015**, *51*, 4447−4450.
(45) Giordanino, F.; Vennestrom, P. N.; Lundegaard, L. F.; Stappen, F. N.; Mossin, S.; Beato, P.; Bordiga, S.; Lamberti, C. Characterization of Cu-exchanged SSZ-13: a comparative FTIR, UV-Vis, and EPR study with Cu-ZSM-5 and Cu-beta with similar Si/Al and Cu/Al ratios. *Dalton Trans.* **2013**, *42*, 12741−12761.

https://doi.org/10.1021/jacs.3c04328
J. Am. Chem. Soc. 2023, 145, 17710−17719

(46) Brezicki, G.; Zheng, J.; Paolucci, C.; Schlögl, R.; Davis, R. J. Effect of the Co-cation on Cu Speciation in Cu-Exchanged Mordenite and ZSM-5 Catalysts for the Oxidation of Methane to Methanol. *ACS Catal.* **2021**, *11*, 4973−4987.

https://doi.org/10.1021/jacs.3c04328
J. Am. Chem. Soc. 2023, 145, 17710−17719